ORIGINAL PAPER

Transportation properties in nanosized LiFePO$_4$ positive electrodes and their effects on the cell performance

**Seungho Yu · Soo Kim · Tae Young Kim ·
Jin Hyun Nam · Won Il Cho**

Abstract To achieve a high energy density for Li-ion batteries, it is important to optimize the electrode thickness and electrode density. It is common to design the electrodes to be thick and dense to achieve a high energy density. However, highly tortuous transport paths in thick and dense electrodes can lead to severe transport losses, which negatively affect the cell performance. In this work, we investigated the effects of varying the electrode thickness and density on lithium ion transport in the electrolytes by means of both experiments and simulations. Both results indicated that an additional capacity loss occurs from the electrode with low porosity because the effective diffusivity decreased in the electrolyte phase. Optimal ranges of the electrode thickness and density (porosity) that can be used to help design high-power LiFePO$_4$/graphite batteries were also suggested in this work.

Keywords Lithium-ion battery · LiFePO$_4$ ·
Electrode density · Electrode thickness · Tortuosity ·
Effective diffusivity

1 Introduction

Electric vehicles (EVs) and hybrid electric vehicles (HEVs) are receiving much attention as clean and efficient

S. Yu · S. Kim · T. Y. Kim · W. I. Cho (✉)
Center for Energy Convergence, Korea Institute of Science and
Technology, 39-1 Hawolgok-dong, Seongbuk-gu, Seoul
136-791, Republic of Korea
e-mail: wonic@kist.re.kr

J. H. Nam (✉)
School of Mechanical and Automotive Engineering, Daegu
University, 15 Naeri-ri, Jinryang-eup, Gyeongsan 712-714,
Republic of Korea
e-mail: jinhnam@gmail.com

alternatives to conventional internal combustion engine vehicles. Accordingly, many studies have been conducted to achieve a high energy density with rechargeable lithium-ion batteries to power EVs and HEVs. Among various active materials (AMs) used for the cathode of lithium-ion batteries, LiFePO$_4$ is a promising candidate for automotive applications because of its high current rate performance, long cycle life, and excellent thermal stability. Recently, researchers improved its low electrical conductivity and ionic diffusivity in the solid state with a carbon coating, metallic element doping, and an AM size reduction [1–6]. In addition, many studies have focused on the electronic and ionic transport processes so that optimized electrode structures could be obtained. In the electrode-scale studies, the key design factors for the optimal electrode performance were identified to be the AM particle size, electrode thickness, AM density (porosity), and electronic conductor fraction [7–11].

To achieve a high energy density for lithium-ion batteries, the electrode thickness and density are the vital design factors at the electrode scale. In general, thick and dense electrode designs provide higher energy densities. However, such electrodes can lead to severe transport limitations due to the tortuous paths in the electrolyte phase. The voltage loss due to the transport limitations is significant in these thick and dense electrodes compared with thin and high-porosity electrodes which allow fast ion transport toward AM particles. The fast voltage drop caused by the ion transport limitation in the thick and dense electrodes can result in the premature termination of the discharge process before full utilization of the AM particles [12, 13].

Numerical modeling is widely used to investigate the effects of the electrode design factors on the battery performance. The mathematical models developed by Newman et al. [14–17] are the most widely used for this

purpose. In fact, Srinivasan and Newman [12, 13] have proposed a one-dimensional (1D) electrochemical model, coupled with a diffusion model inside spherical AM particles, to optimize the electrode design factors of LiFePO$_4$ lithium-ion batteries. These models are constructed based on using the average transport properties, such as the effective diffusivity and conductivity. Proper evaluation of the transport properties to consider the porous electrode structure is very important to accurately predict the electrochemical performance of the lithium-ion batteries and to optimize them effectively.

Tortuosity is a parameter used to describe lithium ion diffusion in the electrolyte phase. In general, the effective diffusivity, D_{eff}, in the porous electrode is evaluated as

$$D_{eff} = \frac{\varepsilon}{\tau}D, \qquad (1)$$

where ε is the porosity of the electrode, τ is the tortuosity, and D (m^2 s^{-1}) is the intrinsic diffusion coefficient in the electrolyte phase. Eq. (1) indicates that the effective diffusivity in the porous electrode is proportional to the transport area, ε, and the elongation of transport length, $1/\tau$. In battery modeling, tortuosity is usually calculated with the Bruggeman coefficient, α, as

$$\tau = \varepsilon^{1-\alpha} \qquad (2)$$

This is the most widely used equation to correlate the porosity and tortuosity.

When fabricating lithium-ion batteries, the density of the electrodes is generally increased to the highest values by compaction of the electrodes using a mechanical roll calendaring press. Mechanical calendaring to compress the electrode is regarded essential to achieving the highest energy densities. However, as the electrode density is increased, the pore space within the electrode is accordingly reduced, creating tortuous transport paths for the electrolytes. As the tortuosity increases, the transport limitation of the electrolyte phase is directly affected. Many recent studies have focused on predicting the tortuosity more accurately to further understand the transport phenomena in the electrodes with low porosities [18–22].

In this study, we investigated the effects of porosity and thickness on the transport properties in a LiFePO$_4$ positive electrode with numerical simulations and experimental studies. First, we conducted a diffusion calculation using a model with 3D structures and predicted the tortuosity as a function of the electrode porosity. From the steady-state diffusion calculation, the tortuosity of electrodes was determined at the various electrode porosities, from which the effective diffusivity was calculated. In addition, electrochemical cell tests were conducted using a LiFePO$_4$ cathode and a natural graphite anode to identify the optimal ranges for the electrode thickness and density.

Our modeling results indicated that additional transport losses occur for electrodes with lower porosities because the effective diffusivity of the electrolytes decreases. Using the experimental results, we found reasonable ranges for the electrode porosity and thickness. In addition, the optimal range for the electrode porosity and thickness needs to be adjusted as the discharge current rate (C-rate) changes. In this work, we predicted the proper electrode porosity and thickness for better designing batteries for various uses at a specific C-rate and confirmed the predictions with experiments to deliver the maximum cell capacity for the optimized performances.

2 Methods

2.1 Numerical

Numerical modeling is used to investigate the transport properties at the 3D porous structure in the cubic domain. The steady state diffusion equation was calculated to obtain the effective transport properties given by

$$\nabla \cdot (D\nabla c) = 0, \qquad (3)$$

where c denotes the concentration (mol m^{-3}). Concentration boundary conditions are applied at the top ($c = 1$ mol m^{-3}) and bottom ($c = 0$ mol m^{-3}). Other boundary conditions are symmetry conditions and the bulk diffusion coefficient is assumed to be 1 m^2 s^{-1}. The effective diffusivity D_{eff} was derived from Ref. [19],

$$\frac{D^{eff}}{D} = \frac{\left[\int_A \nabla c\, dA\right]_{z=L}}{A_s[c(z=L) - c(z=0)]/L} \qquad (4)$$

The porous structure is prepared by means of the random packing method. Random particles were added into the void region until the porosity reaches a desired value. It should be noted that some superposition between the AM particles is allowed when generating a low-porosity structure by the method of random packing; the superposition allowed range was set to <0.5 R. For the acetylene black (AB) particles, we made sure that there was no overlapping with the AM particles or between the AB particles. The design variables to construct porous structures are provided in Table 1. We carefully converted the values typically used in the experiments in terms of volume percent using the materials density (LiFePO$_4$: 3.6 g cm^{-3}, AB: 1.95 g cm^{-3}). In this model, we took the volume percent of the binder to be zero to simplify the structure.

To examine the concentration distribution of porous structures, Eq. (3) is computed by means of the Gauss–Seidel method with up to 500,000 iterations, which is

Table 1 Design variables used for constructing porous structures

Variable	Range
AM:AB size ratio (diameter)	5:1, 10:1, 20:1
AM ratio (vol.%)	40, 45, 50, 55, 60
AB ratio (vol.%)	0, 5, 10, 15

sufficient to achieve solution convergence. The tortuosity of porous structures is then solved through Eq. (5), as given by

$$\tau = \frac{\varepsilon}{D_{eff}} \tag{5}$$

With Eqs. (4) and (5), the effects of porosity on the tortuosity can be analyzed by conducting steady-state diffusion modeling. The average tortuosity is calculated using ten different modeling results in this study. We took the average values of the tortuosity because the tortuosity is not uniquely dependent on the porosity alone. We explored various possibilities for many transport routes by using ten case studies.

2.2 Experimental

The active materials for lithium-ion cell tests (LiFePO$_4$ and graphite) were supplied from SK Innovation Co., Korea. The scanning electron microscope (SEM) images of these powders are shown in Fig. 1, in which the average particle size of LiFePO$_4$ is ~125 nm in radius and that of graphite is ~7 μm. To fabricate the electrodes, slurries were made by mixing each active material (AM) powder with polyvinylidene fluoride (PVDF) binder and acetylene black (AB) conductor powder in N-methyl pyrrolidone (NMP) solvent. The slurries were mixed in a homogenizer for 45 min and then coated onto an Al foil (cathode current collector) and a Cu foil (anode current collector) using a doctor blade, followed by drying in an oven at 80 °C for 4 h. The initial thickness of the electrodes was controlled by the height of the doctor blade.

The amounts of AB powder and PVDF added to the slurries were both 5 wt% for the LiFePO$_4$ electrode. The amount of 5 wt% AB is sufficient for the electrical conductivity due to the carbon coating on the AM particle. The conductivity of the LiFePO$_4$ electrode without AB is 0.42 S m^{-1} and it is increased to 5.52 S m^{-1} at 5 wt% AB. The mixing ratio in the graphite electrode was set to 95 wt% for AM and 5 wt% for PVDF.

For the cell tests, the thickness of the LiFePO$_4$ electrode was varied from 60 to 120 μm. The thickness of the graphite anode was determined to be proportional to the capacity (or the thickness) of the LiFePO$_4$ electrode for the same capacity ratio (1:1) for the full cell tests. The AM
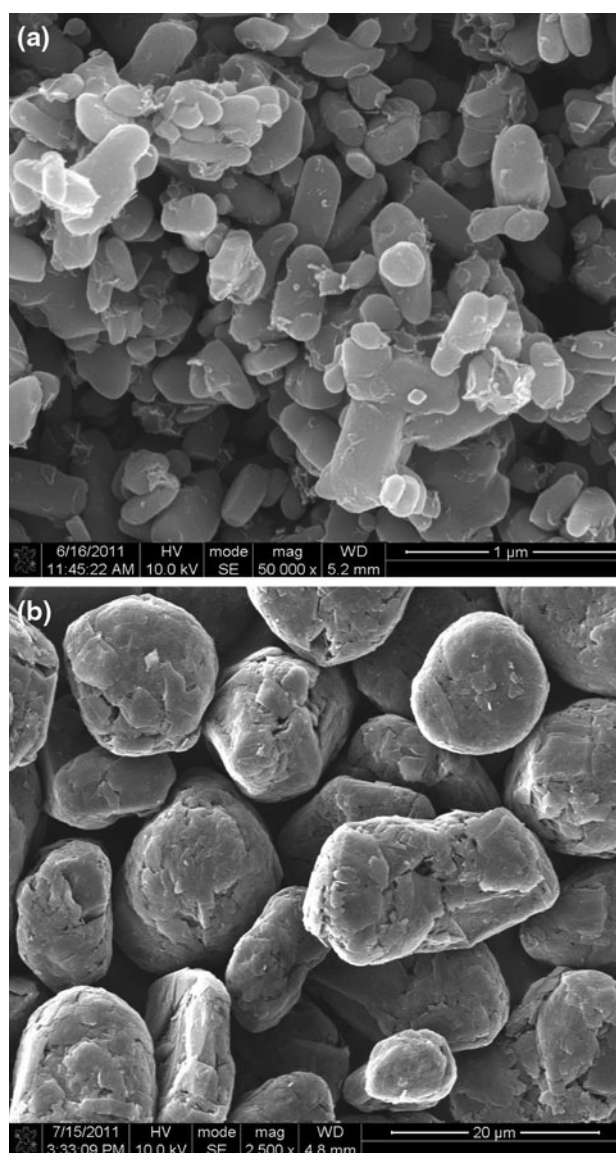

Fig. 1 SEM images of the AM powders. **a** LiFePO$_4$ and **b** graphite

density of the LiFePO$_4$ electrode was calculated after the mechanical calendaring, and typical values of 1.9–2.2 g cm^{-3} were obtained. The AM density of the graphite electrode was set to be relatively lower (approximately 1.4 g cm^{-3}) than the LiFePO$_4$ electrode to avoid the transport loss. After the compaction to the target density, the electrodes were further dried in a vacuum oven at 80 °C for 12 h.

A LiFePO$_4$ electrode and a graphite electrode were then placed in a standard coin cell construction (2032 type) and 1 M LiPF$_6$ in an ethylene carbonate (EC)/dimethyl carbonate (DC)/ethylmethyl carbonate (EMC) solution (1:1:1 vol.%) was added as an electrolyte. The electrochemical behaviors of these cells were tested for several galvanostatic charge/discharge cycles using a battery

Fig. 2 Examples of porous
electrode structures. **a** 5:1, 55,
5; **b** 5:1, 55, 10; **c** 10:1, 55, 5;
and **d** 10:1, 55, 10 (AM:AB size
ratio, AM vol.%, and
AB vol.%)
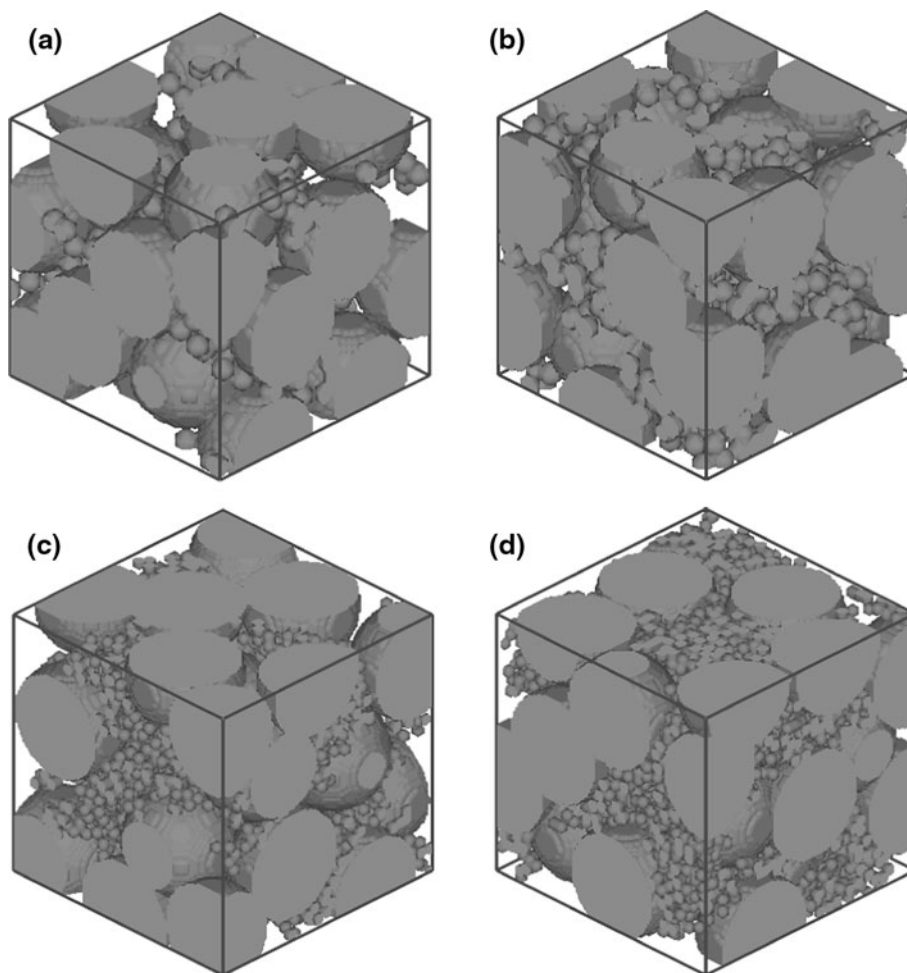
cycler (Maccor 4000, Maccor Inc., USA) with a cut-off
voltage range of 2.5–4.0 V.

3 Results and discussion

3.1 Numerical

The porous structures are created with continuous packing
of the different-sized spheres representing the AM and AB
particles until we reach the target porosity value. The
various structures given in Table 1 are created to investi-
gate the transport properties in the cubic porous domain in
a $100 \times 100 \times 100$ mesh. Among all the structures gen-
erated, we provide four examples in Fig. 2, which illus-
trates (a) 5:1, 55, 5; (b) 5:1, 55, 10; (c) 10:1, 55, 5; and
(d) 10:1, 55, 10 (AM:AB size ratio, AM vol.%, and
AB vol.%). In Fig. 2, it can be observed that as the AM:AB
size ratio and AB vol.% increase, more tortuous paths can
be drawn, which might lead to more severe transport losses
within the electrodes. We only show the AM vol.% of
55 vol.% in Fig. 2 to illustrate the electrode structures with

four different tortuosity values; however, we prepared all
the electrode structures with an AM vol. % of 40, 45, 50,
55, and 60 and an AB vol. % of 0, 5, 10, and 15. Twenty
different calculation results will be provided later in the
discussion section.

Figure 3 illustrates the steady-state concentration pro-
files in the cubic porous domain at 55 vol.% of AM,
(a) 0 vol.% of AB and (c) 5 vol.% of AB. Three XZ planes
($Y = 0.05$, 0.5, and 0.95) from Fig. 3a, c are depicted in
Fig. 3b, d, respectively, to illustrate the internal concen-
tration profiles using the steady-state diffusion equation
given by Eq. (3). Intuitively, the path for the lithium
transport becomes more tortuous because the AM and AB
particles are present. In the porous electrode structures, a
linear concentration gradient is not expected; however,
depending upon the presence of particles, a more irregular
concentration gradient can be induced in our model, as
depicted in Fig. 3. These concentration profiles are used to
acquire the effective diffusivity by Eq. (4) and the tortu-
osity for each porous structure using Eq. (5).

Figure 4 shows the calculation results of the effec-
tive diffusivity values depending on the design values

Fig. 3 Concentration profiles in void regions at 55 vol.% AM. **a** 0 vol.% AB, **b** XZ planes of **a** (Y = 0.05, 0.5, and 0.95), **c** 5 vol.% AB, **d** XZ planes of **c** (Y = 0.05, 0.5, and 0.95)
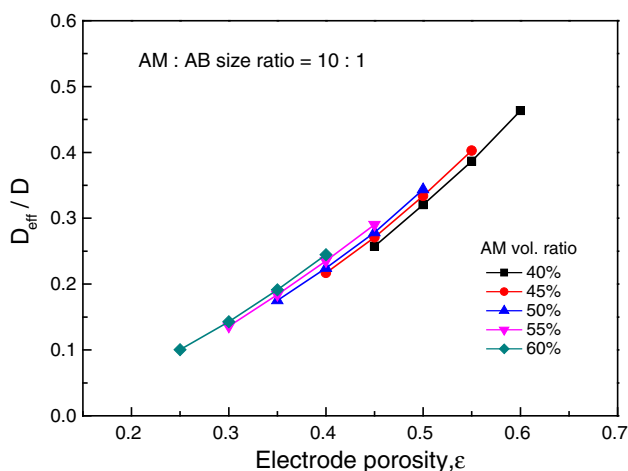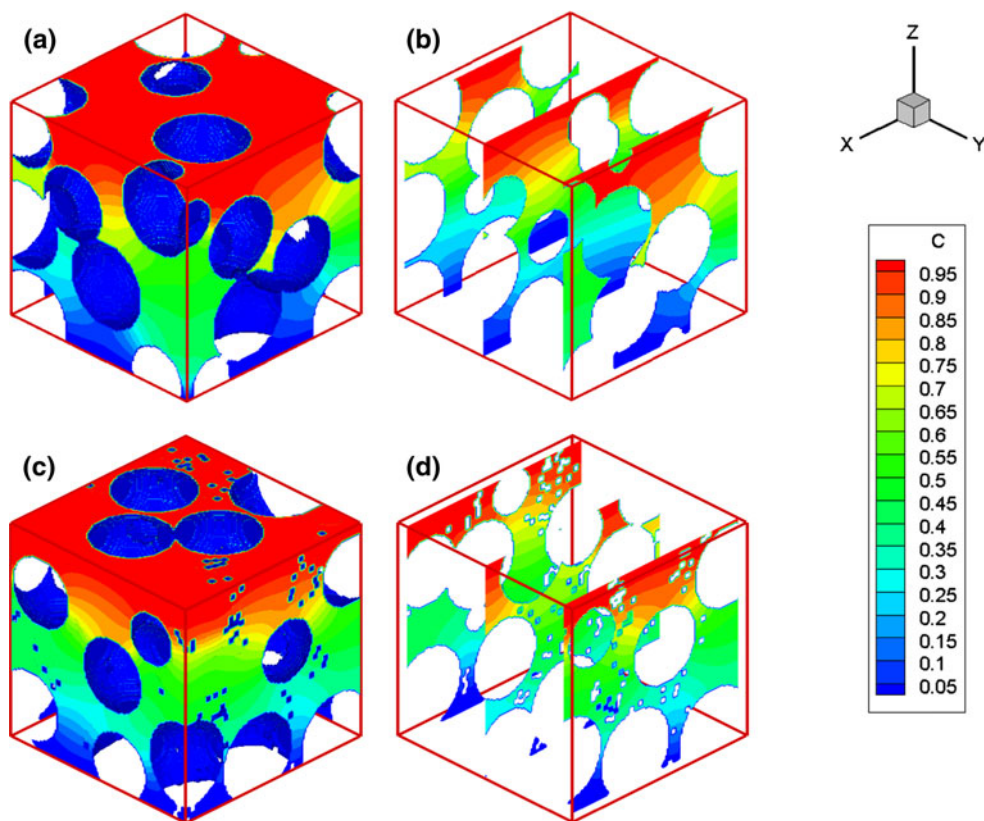

Fig. 4 Effects of porosity on the effective diffusivity at various porous structures

(AM vol.% and AB vol.%) at an AM:AB size ratio of 10:1. The X axis denotes the porosity of the structure domain. The porosity can be calculated as the rest of the volume that remains, excluding the AM vol.% and AB vol.%. For example, when the AM volume ratio is set to 40 vol.%, as the AB ratio increases to 0, 0.05, 0.1, and 0.15, the final electrode porosity is calculated as 0.6, 0.55, 0.5, and 0.45, respectively. As shown in Fig. 4, the effective diffusivity is rapidly reduced to 0.2 as the porosity is decreased to 0.35.

Because porosity values of 0.3–0.35 are typical ranges for commercial electrodes, we note that the transport loss is a major concern that directly reduces the electrochemical performances in lithium-ion batteries based on our calculation results. In addition, we found that the variations in the effective diffusivities are heavily dependent upon the final electrode porosity; however, the individual volumetric ratios of each AM and AB vol.% do not have a significant effect on the effective diffusivity values. For example, the electrode with 45 AM vol.% and 10 AB vol.% shows very similar effective diffusivities of ~ 0.27 with the electrode with 50 AM vol. % and 5 AB vol.%, and both electrodes have the same porosity.

Figure 5 provides the tortuosity values at various porosity structures. The tortuosity of each structure is determined with our effective diffusivity values using Eq. (5). It is illustrated in Fig. 5 that the tortuosity sharply increases when the porosity values are below 0.4. Transport loss can cause dominant voltage loss in the lithium-ion battery with a low-porosity electrode. According to Fongy et al. [11], as the porosity reaches values under 0.35, the cell performance appears to be greatly restricted by the diffusion of lithium ions in the electrolytes. Fongy et al. demonstrated that decreasing the porosity below ~ 0.3 can also cause severe ionic transport limitations. Our calculation results to obtain the effective diffusivity and tortuosity in Figs. 4 and 5 agree with these findings for the low-
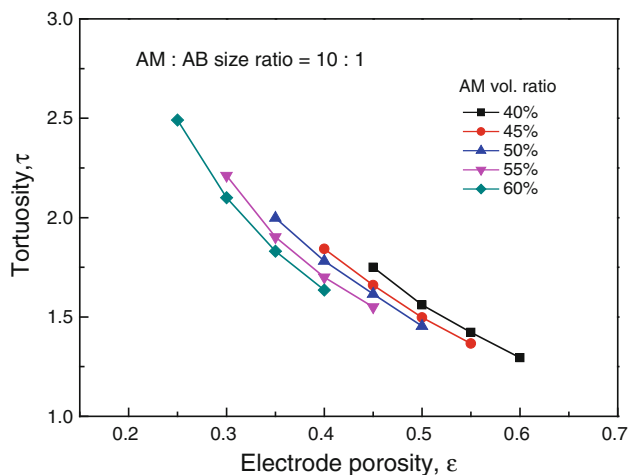
Fig. 5 Effects of porosity on the tortuosity at various porous structures

AM vol.% of 40, 50, and 60 and the AB vol.% of 0, 5, 10, and 15 in each case. In Fig. 6, all the lines represent the AM:AB ratio of 10:1, and all the dots represent the AM:AB ratio of 20:1. In addition, the black-colored objects indicate the AM 40 vol.%, the red-colored objects indicate the AM 50 vol.%, and the blue-colored objects indicate the AM 60 vol.%. As we calculated in Fig. 6, there are no differences in the transport properties when varying the AM:AB size from 10:1 to 20:1 for all AM ratios. This implies that the electrolyte transport is not significantly impeded by the AM:AB size ratio. Rather, the electrode porosity directly affects the transport phenomenon.

Figure 7 compares our calculated tortuosity values with two graphs derived from Bruggeman's equation, Eq. (2). This relation is an empirical model that relates the porosity with the effective diffusivity. In many studies modeling lithium-ion batteries, the effective diffusivity has been calculated using a Bruggeman's coefficient of 1.5. Our calculated tortuosity values from the computational model fit very well in between two dotted lines representing Bruggeman's coefficients of 1.5 and 1.7. To summarize our modeling results, varying the porosity is the primary factor that most significantly affects the transport properties, while the AB ratio and the AM size are negligible compared with the porosities. In particular, electrode structures with a low porosity below 0.3 should be avoided to prevent additional transport losses. To achieve a high power density and avoid transport losses, we suggest that electrodes with a porosity of approximately 0.3 be used to maximize the cell performance.

3.2 Cell test

Based on the modeling results, the porosity of 0.3 is the most favorable for the lithium-ion battery design, which

porosity structures. Unlike the previous work performed by Fongy et al., which predicted the ionic limitations based on the experimental results, we visualized the ionic diffusion limitation in the electrode structures generated by the 3D computational simulations. Again, it can be observed in Fig. 5 that the AB ratio does not significantly affect the transport properties, such as the effective diffusivity and tortuosity. When the porosity of the structures remains the same, more transport losses can be caused when more AB particles are incorporated; however, the effect on the transport properties is not as significant as the effect of varying the porosity.

Finally, we report that the changes in the AM size also have a negligible effect on the transport properties, as illustrated in Fig. 6. In this case, we set the AM vol.% to be 10 and 20 times the AB vol.% for these calculations. In addition, we prepared all the electrode structures with the
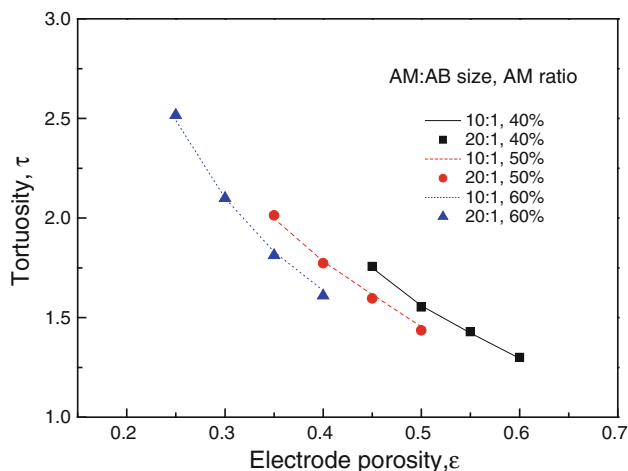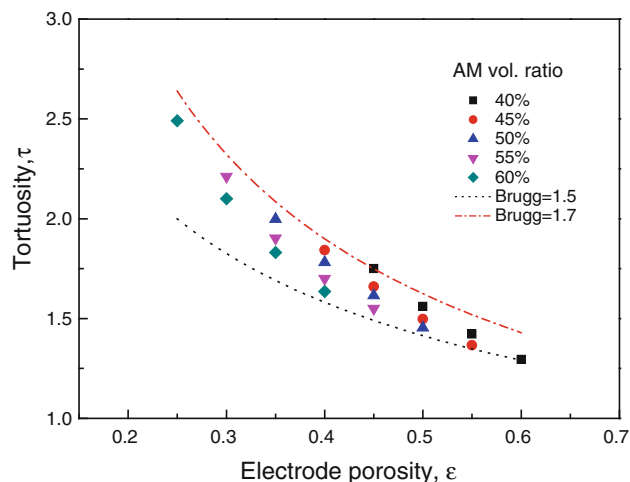

Fig. 6 Effects of the AM size on the tortuosity at various porous structures

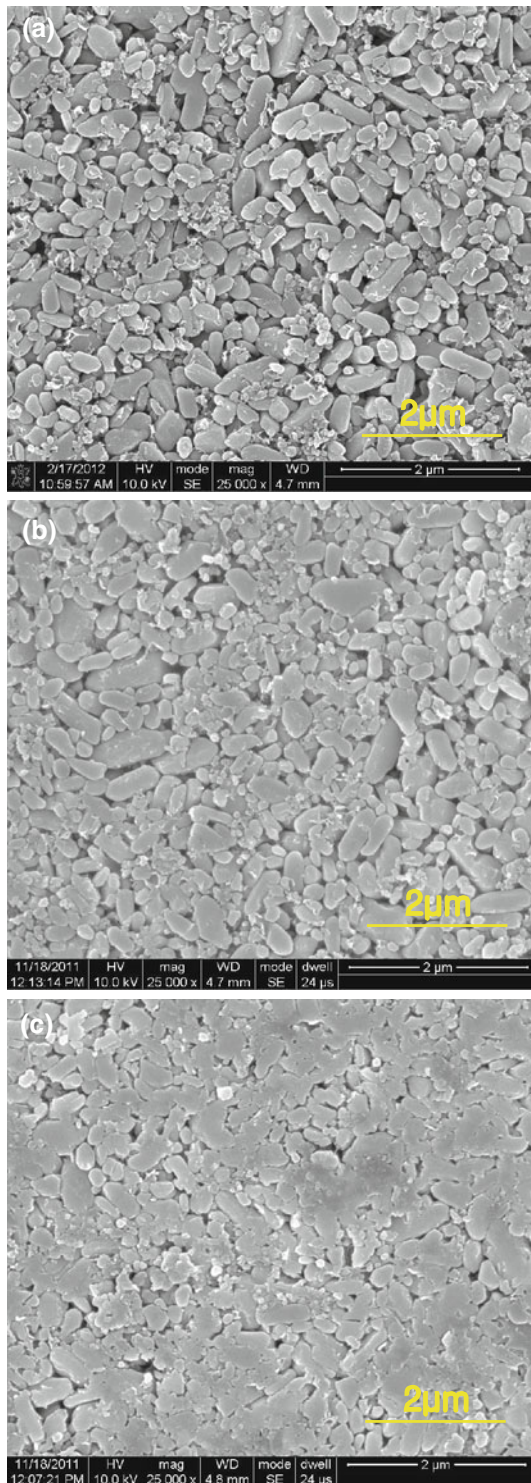**Fig. 7** Porosity-tortuosity relationship of the modeling results in comparison with two Bruggeman equations

Fig. 8 SEM images of the LiFePO$_4$ electrodes at various AM densities. **a** 1.95 g cm^{-3}, **b** 2.04 g cm^{-3}, and **c** 2.17 g cm^{-3}

Fig. 9 FIB-SEM images of the LiFePO$_4$ electrodes at various AM densities. **a** 2.04 g cm^{-3} and **b** 2.17 g cm^{-3}

corresponds to an AM density (AM mass per electrode volume) of 2.05 g cm^{-3}. Figure 8 illustrates the SEM images ($\times$25,000) of the LiFePO$_4$ electrodes, where the AM densities are 1.94, 2.05, and 2.17 g cm^{-3}. Figure 8 indicates that pore spaces decrease and transport paths
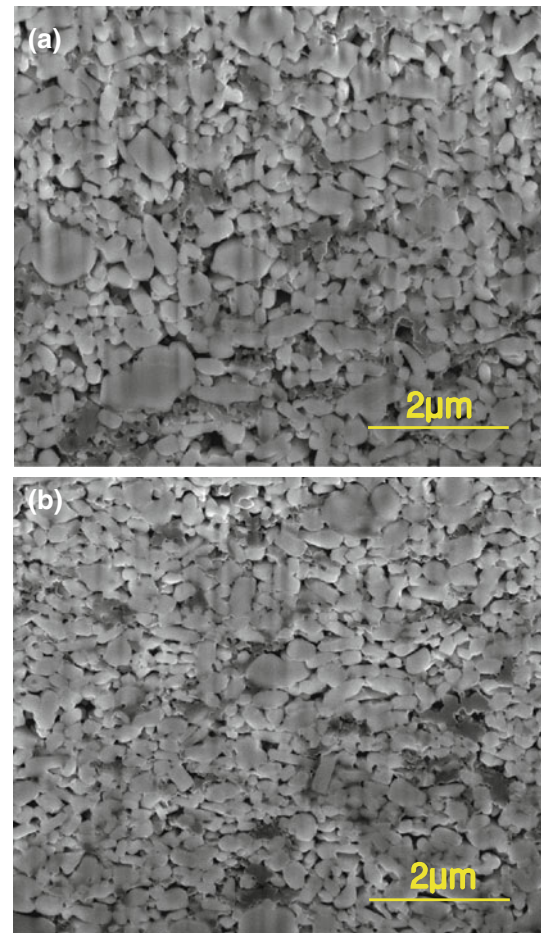
become tortuous when the AM density increases. The performance loss due to the transport limitation can be pictured with these SEM images. Ion transport in the liquid phase is believed to be difficult in these dense electrodes, and thus ionic transport limitation is expected to be the dominant factor determining the capacity loss. An AM density of 2.17 g cm^{-3} is a relatively high value, which requires approximately 40 % compression from its initial electrode thickness.

The porous structure of the electrode can also be observed by the focused ion beam (FIB) technique. Figure 9 describes the FIB-SEM images ($\times$25,000) of the LiFePO$_4$ electrodes in which the AM densities are 2.05 and 2.17 g cm^{-3}. FIB-SEM images present the structure of the electrode, including the ionic transport path and the composition between AM and AB. As mentioned above, the FIB-SEM images show that the pore spaces decrease and the transport paths become tortuous when the AM density increases.

Electrochemical tests are conducted to find the critical values of electrode thickness and density and investigate
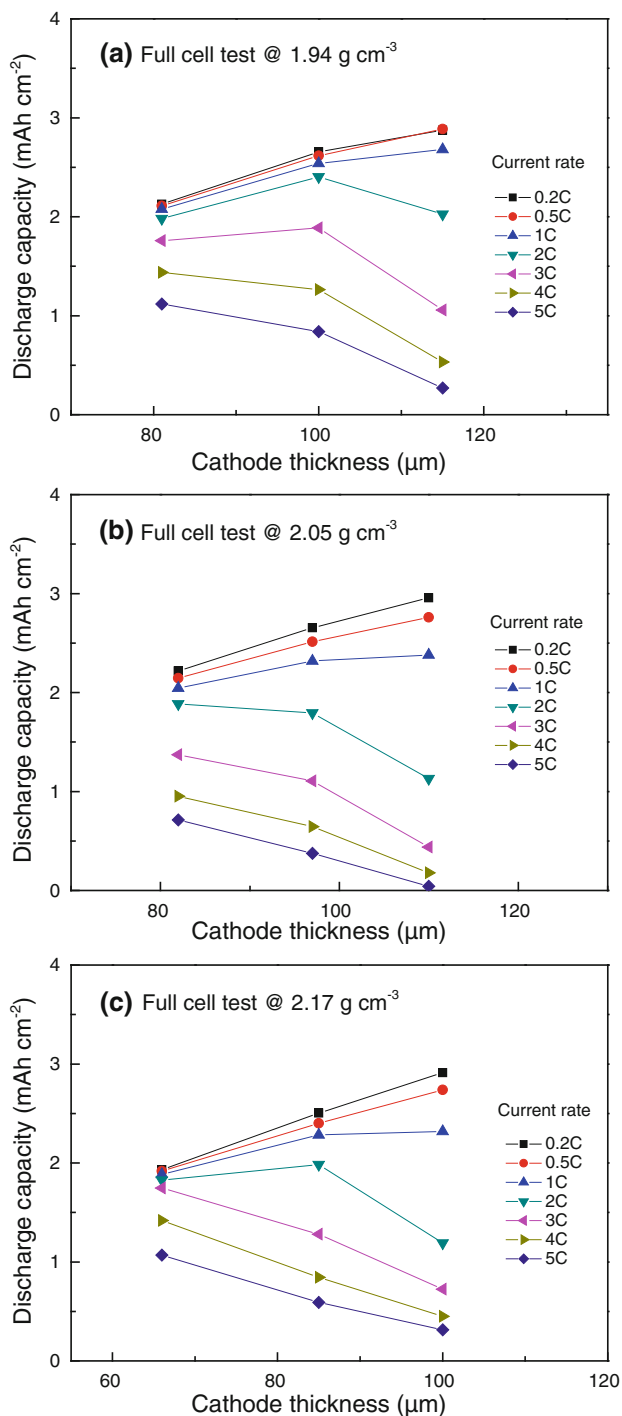
Fig. 10 Discharge capacity per unit area (mAh cm^{-2}) at various cathode thicknesses and current rates. **a** 1.94 g cm^{-3}, **b** 2.05 g cm^{-3}, and **c** 2.17 g cm^{-3}

Fig. 11 Discharge curves of the LiFePO$_4$/graphite full cells at various AM density and current rates. **a** 0.2 C, **b** 1 C, and **c** 2 C

the transport limitation at the thick and dense electrodes. Typically, it is crucial to design thick and dense electrodes to maximize the energy density; however, the modeling work shows the transport limitation of the low-porosity electrode. Therefore, a cell test was conducted to find the optimum thickness and density that does not experience a
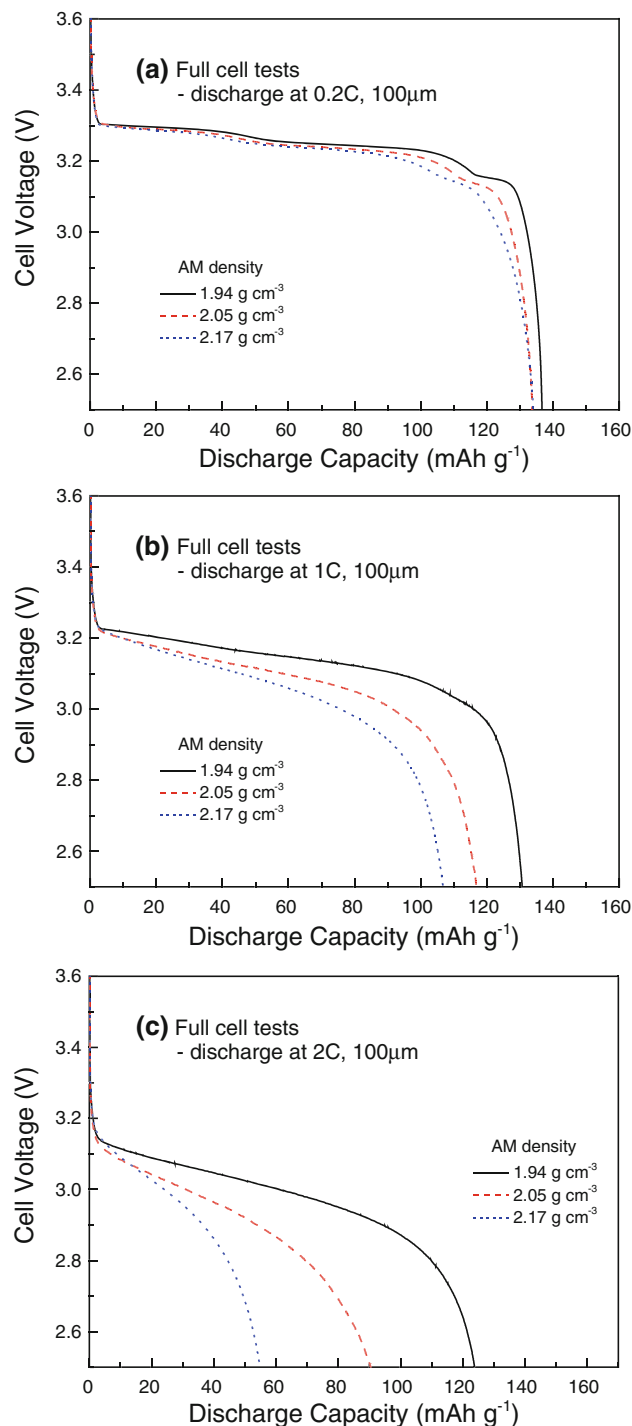
serious transport loss. The thickness range of 60–120 μm is investigated with respect to the current rate at various AM densities in the cathode.

Figure 10 illustrates the discharge capacity per unit area (mAh cm^{-2}) at various cathode thicknesses and current rates: (a) 1.94 g cm^{-3}, (b) 2.05 g cm^{-3}, and (c) 2.17 g cm^{-3}. In

general, the discharge capacity increases proportional to the cathode thickness. As the thickness increases, however, the discharge capacity starts to decrease due to the additional voltage loss. At low current rates (<1 C), the discharge capacity increases proportional to the cathode thickness. Therefore, thick and dense electrodes can be designed to obtain a high discharge capacity without severe transport loss. At 0.2 C, the voltage losses are negligible with respect to the current rate for thicknesses less than 120 μm. However, at high current rates (≥2 C), the discharge capacity shows serious degradation loss when the electrode thickness exceeds 80 μm. This capacity loss is believed to be voltage loss due to the diffusion limitation. Therefore, it is important to use the optimized electrode to maintain a high discharge capacity at high current rates.

Under a 2 C current rate, the optimized thicknesses are approximately 105, 95, and 85 μm at 1.94, 2.05, and 2.17 g cm^{-3}, respectively. At these thicknesses, the discharge capacities are approximately 2.55, 2.3, and 2.3 mAh cm^{-2} at a 1 C current rate and 2.25, 1.85, and 1.95 mAh cm^{-2} at a 2 C current rate. A dense electrode shows more discharge capacity loss as the current rate increases at the optimized thickness for each AM density. This means that electrode compression to obtain a high energy density causes more capacity loss for thick electrodes and high current ratios. Therefore, the proper density should be chosen for high current rate use. For the 100-μm cathode, the optimum AM densities are 2.17, 2.05, and 1.94 g cm^{-3} at 0.5, 1, and 2 C current rates, respectively. At these current rates, the discharge capacities are 2.75, 2.4, and 2.3 mAh cm^{-2}, respectively.

Figure 11 presents the discharge voltage curves with respect to 100-μm thickness at various AM densities and current rates: (a) 0.2 C, (b) 1 C, and (c) 2 C. At 0.2 C, the voltage losses are insignificant with respect to the AM density, as shown in Fig. 11a. However, the voltage drops and the capacity loss increases at high current rates due to the transport limitation. In Fig. 11b, c discharge curves show the severe voltage and capacity losses. This is because the electrode density and thickness exceed the optimal values in Fig. 10. Thus, performing an optimization study for the thickness and density is important to avoid severe discharge capacity losses caused by the transport limitation in the electrolyte.

4 Conclusion

In this study, numerical modeling and detailed experimental tests were performed to investigate the effects of the electrode thickness and density on the ion transport in the electrolyte. First, steady-state diffusion modeling was conducted to obtain the effective transport properties and tortuosity at the various porous structures. The modeling results indicated that a low-porosity electrode reduced the effective diffusivity and conductivity and increased tortuosity. Below a porosity of 0.3, the ionic transport loss is the dominant factor determining the capacity loss. The SEM images also indicate that a dense electrode can cause additional transport losses by reducing the pore space and transport paths.

Based on modeling predictions, full cell tests were conducted to examine the transport limitation in thick and dense electrodes. Electrochemical tests showed that thick and dense electrodes led to a rapid voltage drop when the values exceeded the optimal values. Under a 2 C current rate, which is the typical operation condition, the optimized thicknesses are ~105, 95, and 85 μm at 1.94, 2.05, and 2.17 g cm^{-3}, respectively. In the case of AM density, the proper density should be chosen for high current rate use cases. At the 100-μm cathode, the optimum AM densities are 2.17, 2.05, and 1.94 g cm^{-3} at 0.5, 1, and 2 C current rate, respectively. These optimal ranges for the electrode porosity and thickness can be used to design high-capacity LiFePO$_4$/graphite batteries without severe ionic transport limitations.

References

1. Huang H, Yin SC, Nazar LF (2001) Approaching theoretical capacity of LiFePO$_4$ at room temperature at high rates. Electrochem Solid-State Lett 4:A170
2. Chen Z, Dahn JR (2002) Reducing carbon in LiFePO$_4$/C composite electrodes to maximize specific energy, volumetric energy, and tap density. J Electrochem Soc 149:A1184
3. Chung SY, Bloking JT, Chiang YM (2002) Electronically conductive phospho-olivines as lithium storage electrodes. Nat Mater 1:123
4. Wang D, Li H, Shi S, Huang X, Chen L (2005) Improving the rate performance of LiFePO$_4$ by Fe-site doping. Electrochim Acta 50:2955
5. Shi S, Liu L, Ouyang C, Wang DS, Wang Z, Chen L, Huang X (2003) First-principles study of Li ion diffusion in LiFePO$_4$. Phys Rev B 68:195108
6. Dominko R, Bele M, Goupil JM, Gaberscek M, Hanzel D, Arcon I, Jamnik J (2007) Wired porous cathode materials: a novel concept for synthesis of LiFePO4. Chem Mater 19:2960
7. Gaberscek M (2009) Towards optimized preparation of cathode materials: how can modeling and concepts be used in practice. J Power Sources 189:22
8. Chen YH, Wang CW, Zhang X, Sastry AM (2010) Porous cathode optimization for lithium cells: ionic and electronic conductivity, capacity, and selection of materials. J Power Sources 195:2851
9. Awarkea A, Lauerb S, Pischingera S, Wittlera M (2011) Percolation-tunneling modeling for the study of the electric conductivity in LiFePO$_4$ based Li-ion battery cathodes. J Power Sources 196:405

10. Yu DYW, Donoue K, Inoue T, Fujimoto M, Fujitani S (2006) Effect of electrode parameters on LiFePO$_4$ cathodes. J Electrochem Soc 153:A835

11. Fongy C, Gaillot AC, Jouanneau S, Guyomard D, Lestriez B (2010) Ionic vs electronic power limitations and analysis of the fraction of wired grains in LiFePO$_4$ composite electrodes. J Electrochem Soc 157:A885

12. Srinivasan V, Newman J (2004) Discharge model for the lithium iron-phosphate electrode. J Electrochem Soc 151:A1517

13. Srinivasan V, Newman J (2004) Design and optimization of a natural graphite/iron phosphate lithium-ion cell. J Electrochem Soc 151:A1530

14. Doyle M, Fuller TF, Newman J (1993) Modeling of galvanostatic charge and discharge of the lithium/polymer/insertion cell. J Electrochem Soc 140:1526

15. Fuller TF, Doyle M, Newman J (1994) Simulation and optimization of the dual lithium ion insertion cell. J Electrochem Soc 141:1

16. Fuller TF, Doyle M, Newman J (1994) Relaxation phenomena in lithium-ion-insertion cells. J Electrochem Soc 141:982

17. Doyle M, Newman J (1996) Comparison of modeling predictions with experimental data from plastic lithium ion cells. J Electrochem Soc 143:1890

18. Shearing PR, Howard LE, Jørgensen PS, Brandon NP, Harris SJ (2010) Characterization of the 3-dimensional microstructure of a graphite negative electrode from a Li-ion battery. Electrochem Commun 12:374

19. Gupta A, Seo JH, Zhang X, Du W, Sastry AM, Shyy W (2011) Effective transport properties of LiMn$_2$O$_4$ electrode via particle-scale modeling. J Electrochem Soc 158:A487

20. Kehrwald D, Shearing PR, Brandon NP, Sinha PK, Harris SJ (2011) Local tortuosity inhomogeneities in a lithium battery composite electrode. J Electrochem Soc 158:A1393

21. Thorat IV, Stephenson DE, Zacharias NA, Zaghib K, Harb JN, Wheeler DR (2009) Quantifying tortuosity in porous Li-ion battery materials. J Power Sources 188:592

22. Stephenson DE, Walker BC, Skelton CB, Gorzkowski EP, Rowenhorst DJ, Wheeler DR (2011) Modeling 3D microstructure and ion transport in porous Li-ion battery electrodes. J Electrochem Soc 158:A781